

INORGANIC CHEMISTRY

FRONTIERS



CHINESE
CHEMICAL
SOCIETY



ROYAL SOCIETY
OF CHEMISTRY





rsc.li/frontiers-inorganic

RESEARCH ARTICLE

[View Article Online](#)
[View Journal](#) | [View Issue](#)

 Cite this: *Inorg. Chem. Front.*, 2022, **9**, 4850

2-Dimensional rare earth metal–organic frameworks based on a hexanuclear secondary building unit as efficient detectors for vapours of nitroaromatics and volatile organic compounds†

 Nikos Panagiotou, ^a Francisco García Moscoso, ^b Tânia Lopes-Costa,^b José María Pedrosa ^{*b} and Anastasios J. Tasiopoulos ^{*a}

The synthesis, characterisation and capability to selectively detect vapours of volatile organic compounds (VOCs) and nitroaromatic explosives of a new family of 2-dimensional rare earth (RE) MOFs based on a hexanuclear (RE³⁺)₆ secondary building unit (SBU) is reported. The reaction of RE(NO₃)₃ with 4,4'-sulfonyldibenzoic acid (H₂SDBA) in the presence of 2-fluorobenzoic acid (HFBA) in DMF/MeOH at 100 °C afforded compound [RE₆(μ₃-OH/F)₈(SDBA)₄(NO₃)₂(H₂O)₆]_n (**UCY-15**(RE); RE: Y, Eu, Gd, Tb, Dy, Ho, Er). The structure of **UCY-15**(RE) comprises a microporous 8-connected 2D network based on a (RE³⁺)₆ SBU and the angular dicarboxylate ligand SDBA²⁻ and contains rhombic channels along b and c axes. Gas sorption studies on activated **UCY-15**(Y) indicated a moderate BET surface area of 417 m² g⁻¹. Photoluminescence (PL) studies in the visible region of **UCY-15**(RE) (RE: Y, Eu, Gd, Tb) revealed that SDBA²⁻ is able to sensitize Eu³⁺ and Tb³⁺ ions. Thin films of **UCY-15**(RE) (RE: Y, Eu, Tb) embedded in polydimethylsiloxane (PDMS) were fabricated and evaluated for their sensing capability for vapours of selected VOCs and nitroaromatic compounds revealing different response to each analyte tested. A series of trimetallic analogues **UCY-15**(Y_{100-x-y}Eu_xTb_y) (x, y = 5, 7.5, 10) were prepared aiming to superior sensing materials that combine the PL signals of **UCY-15**(Y), **UCY-15**(Eu) and **UCY-15**(Tb). The analogue **UCY-15**(Y_{87.5}Eu_{7.5}Tb₅) achieved the emission of white light whereas **UCY-15**(Y_{87.5}Eu₅Tb_{7.5})@PDMS films were shown to selectively recognize the tested analytes. Overall, this work highlights the capability of microporous 2D MOFs containing highly accessible emissive centers to recognise vapours of selected analytes.

 Received 13th April 2022,
 Accepted 9th June 2022
 DOI: 10.1039/d2qi00799a
rsc.li/frontiers-inorganic

Introduction

During the past couple of decades materials based on Metal–Organic frameworks (MOFs) are continuously being considered for several applications.¹ Gas storage/separation,^{2–5} catalysis,^{6,7} sensing^{8,9} and removal of pollutants from the environment¹⁰ are among the most prominent applications of MOFs in areas of global interest. The exploding progress in the synthesis of functional MOFs allows the design of materials exhibiting the desired characteristics for the targeted application. For example, by utilizing the molecular building block

(MBB) approach, MOFs with varying network topologies and structural characteristics can be readily designed and synthesized¹¹ giving rise to materials with a plethora of different metal ions, organic ligands, secondary building units (SBUs), functional groups, network topologies, *etc.* Significant attention is focused towards MOFs based on Y³⁺ and trivalent lanthanide ions (Ln³⁺) also collectively referred to as rare earth ions (RE³⁺) because they often exhibit interesting properties.¹² In particular, RE³⁺ MOFs containing emissive metal ions such as Tb³⁺ and Eu³⁺ have been widely employed in photoluminescence (PL) – based sensing applications.^{13–17} Such materials often exhibit attractive features including their porous structures, enabling them to host various prospective analytes, and the presence of multiple emissive moieties, which can act as reporter groups by changing their PL properties upon interaction with guest species.^{18–21} Thus, RE³⁺ MOFs have been utilized as temperature sensors^{13,22,23} and also for the detection, of ions,^{24–28} humidity,²⁹ organic pollutants,³⁰ and nitroaromatics.^{14,31,32} In addition RE³⁺-MOFs have also successfully employed in the detection of various analytes

^aDepartment of Chemistry, University of Cyprus, 1678 Nicosia, Cyprus.
 E-mail: atasio@ucy.ac.cy

^bDepartment of Physical, Chemical and Natural Systems, Universidad Pablo de Olavide, 41013 Seville, Spain. E-mail: jmpedpoy@upo.es

† Electronic supplementary information (ESI) available: Experimental details and figures/tables related to the structural and physicochemical characterisation of the reported compounds. CCDC 2165648–2165653. For ESI and crystallographic data in CIF or other electronic format see DOI: <https://doi.org/10.1039/d2qi00799a>

in the gas phase.^{33–37} However, unlike sensing in liquid media, the preparation of a MOF-based gas sensor is a challenging task because it requires an optically inert platform able to support the MOF crystals and to provide good accessibility of the cages to the incoming gaseous analyte.³⁸ In this sense, embedment of the MOF crystals into thin films of polymeric matrices has shown to be a practical and useful approach for this goal.^{39,40} Focusing on gas sensors exhibiting improved sensitivity and selectivity towards target analytes that are very important for the protection of the society from toxic pollutants and terrorist attacks, polymeric films including RE³⁺-MOFs have been used to detect a number of molecular species including explosives,¹⁵ NO₂¹⁶ and VOCs.²⁵

The stability of MOFs has been one of the major issues for these materials. However, the synthesis of a Zr⁴⁺ MOF based on a hexanuclear [Zr₆(μ₃-O)₄(μ₃-OH)₄(RCOO)₁₂] SBU, called UiO-66⁴¹ unlocked many possibilities for MOFs, since UiO-66 displays significant thermal and chemical stability.^{42,43} This discovery triggered intense research efforts targeting the isolation of other MOFs containing a (Mⁿ⁺)₆ SBU.⁴⁴ As a result, many MOFs based on the above mentioned SBU containing hard metal ions including RE³⁺,⁴⁵ Ce⁴⁺,⁴⁶ Th⁴⁺,^{46,47} and U⁴⁺,⁴⁷ have been synthesized. The isolation of RE³⁺ MOFs based on hexanuclear or more generally polynuclear SBUs requires the use of a carboxylic acid in the reaction mixture such as 2-fluorobenzoic acid (HFBA)⁴⁸ (or 2,6-difluorobenzoic acid (HF₂BA))⁴⁹ which acts as modulator preventing the formation of 1-D RE³⁺ chain SBUs.⁴⁸ We recently focused our attention on the synthesis of novel Zr⁴⁺ or RE³⁺ MOFs containing the hexanuclear SBU targeting to chemically stable MOFs that could be used for the removal and detection of various organic and inorganic species. Moreover, we utilized commercially available angular dicarboxylates possessing different functional groups to investigate the effect of such ligands in the structure and properties of the resulting MOFs. These efforts afforded 2D-8c-Zr-MOFs with the ligands H₂HFPBBA (4,4'-(hexafluoroisopropylidene) bis(benzoic acid)) (compound UCY-13) and H₂OBA (4,4'-oxybis(benzoic acid)) (compound UCY-14) that were stable in aqueous media, displayed appreciable internal surface areas and exhibited exceptional U^{VI}O₂²⁺ sorption capability and selectivity that was attributed to complexation of the U^{VI}O₂²⁺ ion to the terminal hydroxy/water molecules of these MOFs.⁵⁰ In fact, these findings triggered our interest on the synthesis, characterisation and applications of 2D MOFs. This class of compounds can combine the advantages of 2D materials and the interesting properties of MOFs leading to advanced materials with important potential applications in gas sorption/separation, sorption of various organic and inorganic molecules, sensing and catalysis.^{51,52} The advantages that make 2D MOFs attractive for several applications include their easily accessible metal sites and functional groups, enhanced chemical activity, mechanical flexibility, optical transparency, high porosity and significant separation capability as a result of their thin layered structures.^{51,52}

We thus, targeted the isolation of the analogous 2D MOFs of UCY-13 and UCY-14 based on RE³⁺ ions. However, the use

of the angular dicarboxylic ligand H₂OBA (present in UCY-14) afforded a 12-c anionic **pcu**-MOF which proved to be a selective sensor for Cd²⁺ through an ion exchange mechanism.⁵³ Note that apart from the above mentioned MOFs, a number of (RE³⁺)₆-MOFs have been employed for sensing various analytes such as metal ions,^{53–55} NO_x⁵⁶ and small organic molecules^{54,55,57} as well as temperature.^{23,58} In any case, it is not surprising that the use of H₂OBA in the RE³⁺ MOF chemistry led to a high connectivity MOF instead of the 8-c RE³⁺ analogue of UCY-13 and UCY-14 since it is already documented that most (RE³⁺)₆-MOFs display higher connectivity than their (Zr⁴⁺)₆-MOF counterparts due to the flexible coordination environment of RE³⁺ ions compared to the fixed coordination sphere of Zr⁴⁺ ions.⁵⁹ As a result, low-connectivity (RE³⁺)₆-MOFs with 8- or 6-connected SBUs are rather rare.

We herein report the synthesis and characterisation of a new family of 2D MOFs based on the angular dicarboxylic acid ligand 4,4'-sulfonyldibenzoic acid (H₂SDBA) with the general formula [RE₆(μ₃-OH/F)₈(SDBA)₄(NO₃)₂(H₂O)₆]_n (UCY-15(RE); RE: Y, Eu, Gd, Tb, Dy, Ho, Er). Compound UCY-15(RE) is the RE³⁺ analogue of UCY-13 comprising a unique example of a microporous 8-connected 2D network based on (RE³⁺)₆ SBU and a very rare example of a 2D RE³⁺ MOFs based on a hexanuclear SBU. Gas sorption studies of UCY-15(Y) indicated a moderate BET surface area of 417 m² g⁻¹. Solid state PL spectra on UCY-15(RE) (RE: Y, Eu, Gd, Tb) and Na₂SDBA indicated that SDBA²⁻ can sensitize both Eu³⁺ and Tb³⁺ ions. Various trimetallic analogues UCY-15(Y_{100-x-y}Eu_xTb_y) (x, y = 5, 7.5, 10) were synthesized to investigate their capability to emit white light, something that was achieved for UCY-15 (Y_{87.5}Eu_{7.5}Tb₅). Moreover, gas sensing PL studies on PDMS based thin films of UCY-15(RE) (RE: Y, Eu, Tb) (UCY-15(RE)@PDMS) indicated a series of different responses of the three MOFs in the presence of various nitroaromatic compounds and VOCs. Finally, PDMS based thin films of a trimetallic analogue UCY-15(Y_{87.5}Eu₅Tb_{7.5}) was shown to combine the responses obtained for each compound into one material allowing the recognition of the tested analytes.

Experimental

Materials

Reagent grade chemicals were obtained from commercial sources (Aldrich, Merck, Alfa Aesar, TCI, *etc.*) and used without further purification. All synthetic procedures were carried out in air. 2,4-Dinitrotoluene (DNT), 1,3-dinitrobenzene (DNB), 2,4,6-trinitrophenol (TNP) and 2,3-dimethyl-2,3-dinitrobutane (DMNB) were purchased from Sigma-Aldrich. 2,4,6-trinitrotoluene (TNT)⁶⁰ and triperoxide triacetone (TATP)⁶¹ were synthesised following procedures reported in the literature. These procedures are included in the ESI.† Poly(dimethylsiloxane) (Synglard® 184) was purchased from Dow Corning. Other chemical reagents and solvents were of analytical grade and used without further purification.

Synthesis

Synthesis of UCY-15(RE) (RE: Y, Eu, Gd, Tb, Dy, Ho, Er). Solid RE(NO₃)₃ (0.15 mmol) was added in one portion to a clear solution of H₂SDBA (0.015 g, 0.05 mmol), HFBA (0.2 g, 1.43 mmol) and HNO₃ (50 μl, 70 mg, 0.77 mmol) in DMF:MeOH (5 ml:0.5 ml) in a 20 ml glass vial and sonicated until complete dissolution of the reactants. The vial was sealed, placed in an oven at 100 °C and left undisturbed for ~5 days. Then it was cooled to room temperature and X-ray quality colourless rhombic plate crystals of UCY-15(RE) were isolated by filtration, washed with DMF (3 × 5 ml) and dried in air. The reaction yields were in the range of 15–20% based on H₂SDBA. Anal. Calcd UCY-15(Y)·10DMF (Y₆S₄F₃O₅₁N₁₂C₈₆H₁₁₉): C 36.17; H 4.20; N 5.89; found: C 36.46; H 4.49; N 5.70. UCY-15(Eu)·14DMF (Eu₆S₄F₃O₅₅N₁₆C₉₈H₁₄₇): C 33.38; H 4.20; N 6.36; found: C 33.72; H 4.52; N 6.61. UCY-15(Gd)·14DMF (Gd₆S₄F₃O₅₅N₁₆C₉₈H₁₄₇): C 33.38; H 4.16; N 6.30; found: C 32.81; H 4.36; N 6.48. UCY-15(Tb)·16DMF (Tb₆S₄F₃O₅₇N₁₈C₁₀₄H₁₆₁): C 33.63; H 4.37; N 6.79; found: C 33.91; H 4.60; N 6.93. UCY-15(Dy)·15DMF (Dy₆S₄F₃O₅₆N₁₇C₁₀₁H₁₅₄): C 33.12; H 4.24; N 6.50; found: C 33.33; H 4.58; N 6.67. UCY-15(Ho)·15DMF (Ho₆S₄F₃O₅₆N₁₇C₁₀₁H₁₅₄): C 32.99; H 4.22; N 6.48; found: C 33.28; H 4.51; N 6.67. UCY-15(Er)·17DMF (Er₆S₄F₃O₅₈N₁₉C₁₀₇H₁₆₈): C 33.49; H 4.41; N 6.94; found: C 33.78; H 4.34; N 6.89.

Synthesis of UCY-15(Y_{100-x-y}Eu_xTb_y) (x, y = 5, 7.5, 10). Calculated amounts from stock solutions of Y(NO₃)₃, Eu(NO₃)₃ and Tb(NO₃)₃ (0.15 M) in DMF were added in the appropriate molar ratios to a clear solution of H₂SDBA (0.015 g, 0.05 mmol), HFBA (0.2 g, 1.43 mmol) and HNO₃ (50 μl, 70 mg, 0.77 mmol) in DMF:MeOH (4 ml:0.5 ml) in a 20 ml glass vial. The vial was sealed, placed in an oven at 100 °C and left undisturbed for ~5 days. Then it was cooled to room temperature and X-ray quality colourless rhombic plate crystals of UCY-15(Y_{100-x-y}Eu_xTb_y) (x, y = 5, 7.5, 10) were isolated by filtration, washed with DMF (3 × 5 ml) and dried in air. The reaction yields were in the range of 10–20% based on H₂SDBA.

UCY-15(RE)@PDMS (RE: Y, Eu, Tb, Y_{87.5}Eu₅Tb_{7.5}) film preparation. 20 mg of each MOF were mixed with a Sylgard® 184 base and the curing agent in a 10:1 weight ratio (1 g and 0.1 g respectively). The mixture was vigorously stirred for 30 minutes. After the complete dispersion of the MOF powder into the polymer matrix, the mixture was spin-coated on a Petri dish at 1000 rpm for 60 s and subsequently put under vacuum for 15 minutes to degas the fresh polymer. Then, it was placed in an oven at 60 °C overnight. The films (mixed matrix membranes, MMMs) were cut and peeled off for characterisation and sensing assays.

Gas sensing assays

The different UCY-15(RE) MOFs were exposed to saturated vapours of six explosives, *i.e.* TNT, TNP, DNT, DNB, DMNB and TATP and five pure volatile organic compounds (VOCs), *i.e.* toluene, ethanol, methylamine, chloroform and hexanal. For the sensing measurements of explosives, the UCY-15(RE)@PDMS films were placed in a glass vial, whose head space

was previously saturated with vapours of a certain quantity of solid explosive (approximately 10 mg), and hermetically closed. Although the main part of the sensing reaction with explosives is expected to take place during the first minutes, the exposure was continued for 48 hours in order to ensure complete saturation.

On the other hand, the exposure to the VOCs was carried out in a shorter time because of the higher vapour pressure of these compounds. In this case, the saturated vapours of each VOC was obtained by bubbling dry N₂ through the pure liquid analyte, resulting in a mixture of N₂ saturated in each VOC. The gas flow rates were controlled using two Bronkhorst® F-201FV mass flow controllers, and the gas flow rate was fixed at 1 L min⁻¹. Then, the gas mixture was introduced in another gas chamber where the samples were previously placed for exposure, which was maintained for 15 minutes.

In both cases, the PL spectra of the UCY-15(RE)@PDMS films were recorded before and after their exposure to the analyte until saturation of the sensing response unless otherwise mentioned.

Physical measurements

Elemental analyses (C, H, N) were performed by the in-house facilities of the University of Cyprus, Chemistry Department. IR spectra were recorded on ATR in the 4000–700 cm⁻¹ range using a Shimadzu Prestige – 21 spectrometer. pXRD patterns were recorded on a Shimadzu 6000 Series X-ray diffractometer (Cu Kα radiation, λ = 1.5418 Å). Thermal stability studies were performed with a Shimadzu TGA 50 thermogravimetric analyzer. ¹H NMR spectra were recorded on a Bruker Avance III 300 MHz spectrometer at 25 °C. Chemical shift values in ¹H NMR and ¹⁹F-NMR spectra were reported in parts per million (ppm). Digestion of the samples (~10 mg) was achieved with 0.5 M KOH in D₂O. Solid state PL measurements for UCY-15(RE) (RE: Y, Eu, Gd, Tb) and UCY-15(Y_{100-x-y}Eu_xTb_y) (x, y = 5, 7.5, 10) were carried out on an Edinburgh Xe900. All spectra were corrected for instrument response using the correction function generated after calibration of the instrument with a standard light source. Appropriate long pass filters were used to remove scattering from the sample and the monochromators.

PL emission and excitation spectra of UCY-15(RE)@PDMS films were recorded with an FLS1000 Photoluminescence Spectrophotometer (Edinburgh Instruments). In addition, X-ray microdiffraction (μ-XRD) patterns of the membranes were collected using a Discover D8 (Bruker) diffractometer with Cu Kα radiation (1.5406 Å, 50 kV, 1000 mA) in the 5°–35° 2θ range with a step of 0.02° per 0.5 s. The shape and size of the MOF particles were examined using a FEI Teneo scanning electron microscope (SEM). The samples for the SEM experiments were prepared by depositing a droplet of an aqueous suspension of the MOF particles onto a copper tap and dried in air. Each sample was then covered with a 5 nm layer of carbon by using a Leica ACE 600 sputter. Semiquantitative elemental analysis was obtained by Scanning electron microscopy-Energy dispersed X-ray spectroscopy (SEM-EDX) using the FEI Teneo microscope.

Gas adsorption

Low Pressure gas sorption measurements were carried out at different temperatures using an Autosorb-iQ3 by Quantachrome system equipped with a cryocooler capable of temperature control from 20 to 320 K. Prior to analysis the as made samples were washed with *N,N*-dimethylformamide four times per day for 1 day and then soaked in MeCN or CHCl₃ 3 times per day for 10 days. Finally, the wet samples were transferred to 6 mm sample cells and activated under dynamic vacuum at room temperature for 18 hours until the outgas rate was less than 2 mTorr min⁻¹. After evacuation, the samples were weighed to obtain the precise mass of the evacuated sample and the cells were transferred to the analysis port of the gas sorption instrument.

Single crystal X-ray crystallography

Single Crystal X-ray diffraction data were collected on a Rigaku Supernova A diffractometer, equipped with a CCD area detector utilizing Cu-K α ($\lambda = 1.5418 \text{ \AA}$) radiation. A suitable crystal was mounted on a Hampton cryoloop with paratone-N oil and transferred to a goniostat where it was cooled for data collection. The structures were solved by direct methods using SHELXT and refined on F^2 using full-matrix least squares using SHELXL14.1.⁶² Software packages used: CrysAlis CCD for data collection, CrysAlis RED for cell refinement and data reduction,⁶³ WINGX for geometric calculations,⁶⁴ and DIAMOND for molecular graphics.⁶⁵ The non-H atoms were treated anisotropically, whereas the aromatic hydrogen atoms were placed in calculated, ideal positions and refined as riding on their respective carbon atoms. Several restraints (DFIX, SIMU, RIGU and DELU) were used to fix the thermal ellipsoids and geometry of the bridging NO₃⁻ ions. Electron density contributions from disordered guest molecules were handled using the SQUEEZE procedure from the PLATON software suite⁶⁶ due to the disordered nature of these molecules. Selected crystal data for UCY-15(RE) (RE: Y, Eu, Gd, Tb, Dy, Ho) are summarized in Table S1 in ESI.† CCDC 2165648–2165653† contain the supplementary crystallographic data for this paper. Full details can be found in the CIF files provided as ESI.†

Results and discussion

Synthesis and crystal structure

The last few years we have been investigating the use of angular dicarboxylic ligands in MOF chemistry targeting to new functional MOFs. These efforts have afforded a series of Cu²⁺ MOFs⁶⁷ as well as two Zr⁴⁺ MOFs, compounds (UCY-13) and (UCY-14).⁵⁰ We have also employed such ligands in RE³⁺ MOF chemistry targeting the isolation of structural analogues of the two Zr⁴⁺ MOFs as well as other functional MOFs.⁵³ Among the various angular dicarboxylic ligands used for this purpose, 4,4'-sulfonyldibenzoic acid (H₂SDBA) has attracted our attention due to its potential to afford functional MOFs. In particular, it is emissive in the visible region of the UV-Vis

spectrum and additionally has stabilized an 8c-(Zr⁴⁺)₆-MOF that was shown to be an efficient sensor for various organic compounds including nitroaromatics.⁶⁸ Consequently, we explored reactions of H₂SDBA with RE³⁺ salts in the presence of HFBA targeting analogues of UCY-13 and UCY-14. These synthetic efforts involved use of various RE³⁺ salt/H₂SDBA molar ratios and reaction conditions (solvent system, addition of concentrated acids and the reaction temperature). Thus, the reaction of RE(NO₃)₃ with H₂SDBA in a 3:1 molar ratio in DMF/MeOH in the presence of ~30 equivalents of HFBA and ~15 equivalents of concentrated HNO₃ at 100 °C for five days afforded colourless rhombic crystals of compound UCY-15(RE) (RE: Y, Eu, Gd, Tb, Dy, Ho, Er). The structure of compound UCY-15(RE) (RE: Y, Eu, Gd, Tb, Dy, Ho) crystallizing in the monoclinic space group *C2/m* contains two crystallographically independent RE³⁺ ions. The experimental pXRD patterns of UCY-15(RE) analogues along with the simulated one of UCY-15 (Y) are shown in Fig. S1 in ESI.† Since the UCY-15(RE) compounds are isostructural, crystallize in the same space group with similar unit cell dimensions and their main difference is the RE³⁺ ion that is present in each structure, we will discuss in detail only the structure of UCY-15(Y). Representations of the structure of UCY-15(Y) are shown in Fig. 1. Y1 ion is coordinated to eight oxygen atoms adopting a square antiprismatic geometry whereas Y2 to nine oxygen atoms adopting a monocapped square antiprismatic geometry.⁶⁹ Specifically, the coordination sphere of Y1 consists of four μ_3 -OH⁻ bridges, two carboxylate oxygen atoms of two bridging SDBA²⁻ ligands, one oxygen atom of a bridging NO₃⁻ ion and a terminal water molecule, whereas the one of Y2 of four μ_3 -OH⁻ bridges, four carboxylate oxygen atoms from four bridging SDBA²⁻ ligands and a terminal water molecule (Fig. S2 and Table S2†). Recent publications concerning RE-MOFs synthesized utilizing HFBA or HF₂BA indicated the existence of μ_3 -F⁻ bridging ions.^{70,71} The existence of F⁻ anions in this compound was confirmed by recording ¹⁹F-NMR spectra of a digested sample of UCY-15 (Y) which indicated the presence of around three F⁻-ions per (Y³⁺)₆ SBU.^{70,71} (Fig. S3–S6†). Overall, the secondary building unit of UCY-15(Y) is a hexanuclear cluster based on a [Y₆(μ_3 -OH⁻/F⁻)₈]¹⁰⁺ structural core in which the Y³⁺ ions occupy the vertices of an octahedron and the μ_3 -OH⁻/F⁻ bridges lie above its faces. Two SDBA²⁻ ligands connect two neighbouring (Y³⁺)₆ SBUs with each carboxylate group linking two Y³⁺ ions of the hexanuclear SBU adopting the common *syn,syn*- η^1 : η^1 : μ coordination mode. As a result, the eight SDBA²⁻ ligands connect the hexanuclear SBU with four other SBUs forming a neutral 2-dimensional nanosheet with ~14 Å thickness. The 2D nanosheets feature two types of rhombic cavities with dimensions ~10 × 19 Å² and ~10 × 12 Å² (Fig. 1a) and are oriented parallel to each other. This parallel packing is achieved through soft hydrogen bonds (C–H...O) involving O atoms of the sulfone groups and C–H moieties of the aromatic rings of SDBA²⁻ ligands belonging to neighbouring 2D nanosheets (Fig. 1b) (O...C distance 3.254 Å).⁷² The parallel packing of the 2D nanosheets leads to inter-layer rhombic channels involving the larger cavities of each layer along the *c*-axis (Fig. 1c),

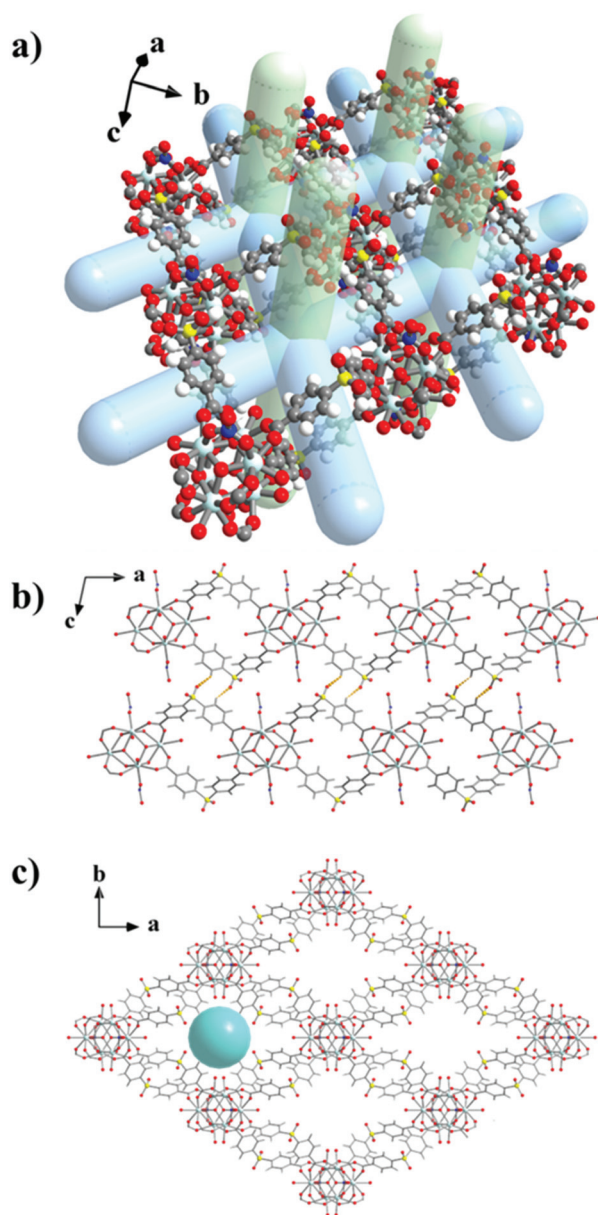


Fig. 1 Representations of: (a) a single nanosheet of **UCY-15(Y)** emphasising on its cavities and channels with the light blue bars being used to indicate the intralayer channels and the light green bars the interlayer channels extending to parallel neighbouring nanosheets, the 2D framework of **UCY-15(Y)** formed along the (b) *b* axis indicating the soft hydrogen bonding interactions (orange dashed bonds) between adjacent nanosheets and (c) *c* axis emphasising on the parallel packing of the 2D nanosheets and the interlayer rhombic channels along this axis. The cyan sphere (shown in c) denotes the pores formed between the parallel layers along *c*-axis. Colour code: Y, light blue; S, yellow; O, red; N, blue; C, grey; H, white.

whereas the smaller cavities form intra-layer channels (Fig. 1b). The solvent accessible volume of the framework corresponds to ~62% of the unit cell volume.

Although several examples of RE^{3+} MOFs based on the hexanuclear SBU have been reported, the vast majority is 3D compounds.^{45,48,49,53,73–76} To the best of our knowledge, com-

pound **UCY-15(RE)** is only the second example of a 2D MOF based on $(\text{RE}^{3+})_6$ -SBU.⁷⁷ The existence of a very limited number of 2D MOFs based on a $(\text{RE}^{3+})_6$ -SBU is rationalized on the basis of the presence of several carboxylate groups connecting the RE^{3+} ions of the SBU due to the extended and flexible coordination sphere of these ions leading to 3D structures. It is pointed out that low connectivity $(\text{RE}^{3+})_n$ ($n = 6, 9$)-SBUs are also known, with most of them being rationally designed and synthesized based on topological aspects.^{71–74} In fact, one of these low connectivity networks and in particular a 6-connected one is the only other example of a 2D framework with a $(\text{RE}^{3+})_6$ SBU.⁷⁷ It is also interesting that **UCY-15(RE)** exhibits analogous structure with a 2D Zr^{4+} MOF we reported recently formulated as $[\text{Zr}_6(\mu_3\text{-O})_4(\mu_3\text{-OH})_4(\text{HFPBBA})_4(\text{OH})_4(\text{H}_2\text{O})_4]_n$ (compound **UCY-13**).⁵⁰

The thermal stability of **UCY-15(RE)** analogues was investigated by means of thermogravimetric analysis (Fig. S7†) and variable temperature pXRD of the as synthesized samples (Fig. S8†). The thermal decomposition of compounds **UCY-15(RE)** proceeds *via* a two-step process. The first step (until ~460–480 °C) is attributed to the removal of the terminal H_2O and lattice DMF molecules. The second mass loss which is completed at ~650 °C is attributed to the decomposition of the ligand SDBA^{2-} . The residual mass at 900 °C corresponds to the rare earth oxide of the corresponding RE^{III} ion (Table S3†). Variable temperature pXRD studies confirm that **UCY-15(Y)** exhibits a significant thermal stability up to high temperatures (>400 °C) (Fig. S8†).

Gas sorption properties

Since **UCY-15(Y)** is stable in low boiling point solvents like MeCN and CHCl_3 (Fig. S9†), the activation of the material was performed through exchange of the lattice and coordinated solvent molecules with these solvents. These studies indicated that **UCY-15(Y)** activated with these solvents (Fig. S10†) displayed similar surface area and pore volume values however, the materials activated in MeCN showed slightly higher values. N_2 sorption measurements at 77 K of **UCY-15(Y)** activated through a solvent exchange process with MeCN, revealed a type-I isotherm typical for microporous solids (Fig. 2), from which the apparent BET area was found to be $417 \text{ m}^2 \text{ g}^{-1}$ (Langmuir, $431 \text{ m}^2 \text{ g}^{-1}$) (Fig. S11 and S12†). The total pore volume value of $0.19 \text{ cm}^3 \text{ g}^{-1}$ at relative pressure, $p/p^0 = 0.99$, is lower compared to the value of $0.61 \text{ cm}^3 \text{ g}^{-1}$ calculated from the crystal structure of **UCY-15(Y)**. Given that the pXRD pattern of the activated sample suggests an intact framework (Fig. S9†), the difference in the pore volume could be explained by the presence of trapped organic molecules within the pores for both compounds. The pore size distribution was calculated using non-local density functional theory (NLDFT) after a successful fitting of the N_2 adsorption isotherm data using a suitable NLDFT kernel (Fig. S13 and S14†). **UCY-15(Y)** shows two major peaks centred at 8.3 Å and 16.3 Å. The larger pore size value cannot be rationalized on the basis of the crystallographic data and is attributed to missing linker defects, which is common in this family of compounds due to the use of

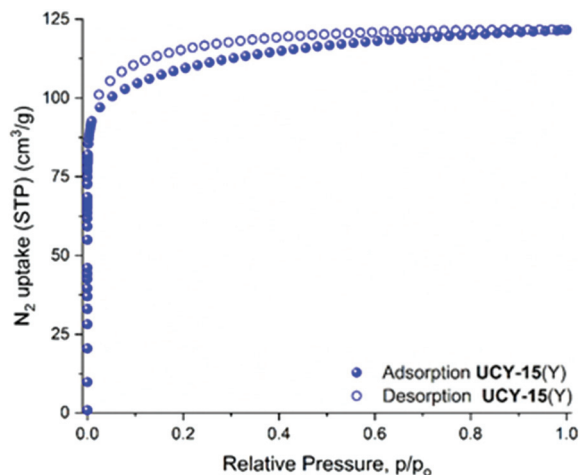


Fig. 2 N₂ adsorption isotherm at 77 K for UCY-15(Y).

modulators. The CO₂ uptake was investigated up to 1 bar at 273 K, 283 K and 298 K (Fig. S15[†]). UCY-15(Y) was found to adsorb 2.3 (10.13 wt%), 1.70 (7.52 wt%) and 1.21 (5.36 wt%) mmol CO₂ g⁻¹ and the isosteric heat of adsorption, Q_{st}^o , was calculated to be 30.3 kJ mol⁻¹ (Fig. S16 and S17[†]).

Photophysical properties

Steady state and time resolved PL spectroscopy studies were performed on microcrystalline samples of UCY-15(RE) (RE: Y, Eu, Gd, Tb) and the ligand. Upon excitation at 338 nm a broad emission band at 427 nm is observed in PL spectra of the ligand Na₂SDBA which is attributed to the $\pi^* \rightarrow \pi$ transition of the ligand (Fig. S18[†]). Further studies included the measurement of the PL spectra of UCY-15(RE) (RE: Y, Gd) where the excitation and emission signals are slightly shifted compared to the corresponding signals of the Na₂SDBA ligand. Specifically, a broad emission band at 433 nm is observed upon excitation at 325 nm for these two compounds which is also attributed to the $\pi^* \rightarrow \pi$ transition of the anion of SDBA²⁻ (Fig. S18[†]). UCY-15(RE) (RE: Eu, Tb) display the characteristic PL spectra of Eu³⁺ and Tb³⁺ ions upon excitation at 302 and 303 nm, respectively. It should be noted that in this region only SDBA²⁻ absorbs light which sensitizes the RE³⁺ ions through energy transfer. In the case of UCY-15(Eu), upon excitation at 302 nm, sharp but weak emission bands are observed at 578, 591, 613, 651 and 699 nm corresponding to $^5D_0 \rightarrow ^7F_J$ ($J = 0, 1, 2, 3$ and 4 , respectively) transitions (Fig. 3a). UCY-15(Tb) displays strong and sharp emission bands at 487, 543, 582 and 620 nm which are attributed to the $^5D_4 \rightarrow ^7F_J$ ($J = 6, 5, 4$ and 3 , respectively) transitions (Fig. 3b).

The difference in intensity of the PL signals of the two compounds UCY-15(Eu) and UCY-15(Tb) is due to the energy difference of the excited T₁ energy state of SDBA²⁻ anion (T₁, 23 095 cm⁻¹; estimated from the emission spectrum of UCY-15(Y)) and the emissive states of Eu³⁺ (5D_0 , 17 200 cm⁻¹) and Tb³⁺ (5D_4 , 20 500 cm⁻¹) ions which is 5895 cm⁻¹ and 2595 cm⁻¹, respectively. Thus, in the case of UCY-15(Eu) the

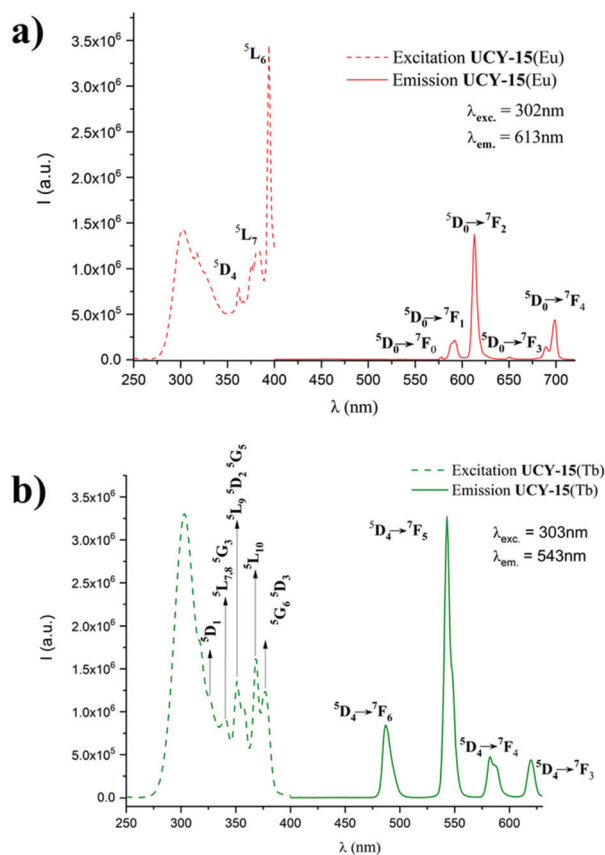


Fig. 3 (a) Solid state excitation spectra ($\lambda_{em} = 613$ nm) and emission ($\lambda_{exc} = 302$ nm) of the as synthesized compound UCY-15(Eu), (b) solid state excitation spectra ($\lambda_{em} = 543$ nm) and emission ($\lambda_{exc} = 303$ nm) of the as synthesized compound UCY-15(Tb).

energy difference is well above the upper limit of 4000 cm⁻¹ for efficient sensitization of Eu³⁺ ion, possibly explaining the weak emission peaks in the PL spectra of UCY-15(Eu), whereas in the case of UCY-15(Tb) the energy difference is slightly above the lower limit of 2500 cm⁻¹ for efficient sensitization of Tb³⁺ ion which implies that energy transfer from the SDBA²⁻ ligand to Tb³⁺ ions is favorable.^{25,78} The excitation spectra of UCY-15(Eu) and UCY-15(Tb), monitored at 613 nm and 543 nm, respectively, display characteristic peaks corresponding to f-f transitions (Fig. 3). Time resolved emission studies on UCY-15(Eu) and UCY-15(Tb) revealed that the PL signals of the rare earth ions show mono-exponential decays with lifetimes of $\tau_{obs}^{Eu} = 1.0$ ms and $\tau_{obs}^{Tb} = 1.4$ ms (Fig. S19[†]). These lifetimes are in agreement with the values obtained for several Eu³⁺ and Tb³⁺ coordination polymers and MOFs.^{79,80} In the case of UCY-15(Eu) we were able to estimate the emission quantum yield of the Eu³⁺ ion, $\Phi_{Eu}^{Eu} = \sim 38\%$ (see ESI[†] for detailed discussion).

Thin film characterisation and sensing studies

The SEM images of a cross-section of the UCY-15(Y)@PDMS based films (Fig. 4a) reveal a homogeneous thickness of 59 μ m for the obtained membranes. In addition, the MOFs particles

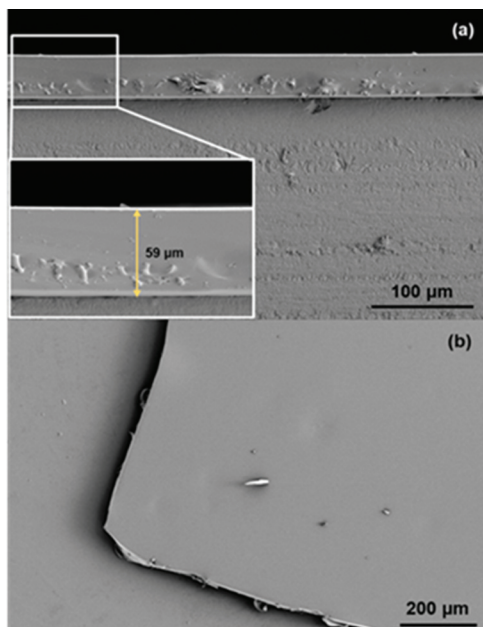


Fig. 4 (a) Cross-section and (b) top-view of a UCY-15(Y)@PDMS membrane.

are totally embedded into the porous PDMS as shown in Fig. 4b. Similar results were obtained for UCY-15(Eu)@PDMS and UCY-15(Tb)@PDMS.

The crystallinity of the MOF, once embedded in the PDMS membrane, was confirmed by μ -XRD (Fig. S20[†]). As can be observed, the diffractogram of UCY-15(Y)@PDMS reveals that the MOF particles remain crystalline after being incorporated into the PDMS membranes since the two low angle peaks can be clearly distinguished from the noise signal of the mainly amorphous PDMS – based films. Furthermore, the amorphous phase around 12° is attributed to the polymeric matrix. Hence, these results prove the existence of the crystalline phase (MOF) in the mixed-matrix membrane (MMM).

The PL emission spectra upon excitation at 325 nm, of UCY-15(Y)@PDMS (blue line), UCY-15(Eu)@PDMS (red line) and UCY-15(Tb)@PDMS (green line) are shown in Fig. 5. As can be seen, the three membranes exhibit the same emission profile as the microcrystalline powder of the corresponding analogues of UCY-15(RE) (RE: Y, Eu, Tb). Moreover, the insets in Fig. 5 illustrate the strong emission of the films, especially of UCY-15(Eu)@PDMS and UCY-15(Tb)@PDMS, when illuminated with UV light (300–375 nm). The microporous structure of UCY-15(RE), that could possibly allow the insertion of various organic molecules into the pores, and the accessibility of the emissive sites due to the 2D nature of this family of MOFs that could lead to intense modifications of the PL signal of the MOF upon exposure to a certain analyte, prompted us to investigate the gas sensing properties of thin films based on these materials. When the UCY-15(RE)@PDMS (RE = Y, Eu, Tb) films were exposed to saturated vapours of TNT, a substantial quenching was achieved in all cases, as shown in Fig. 6.

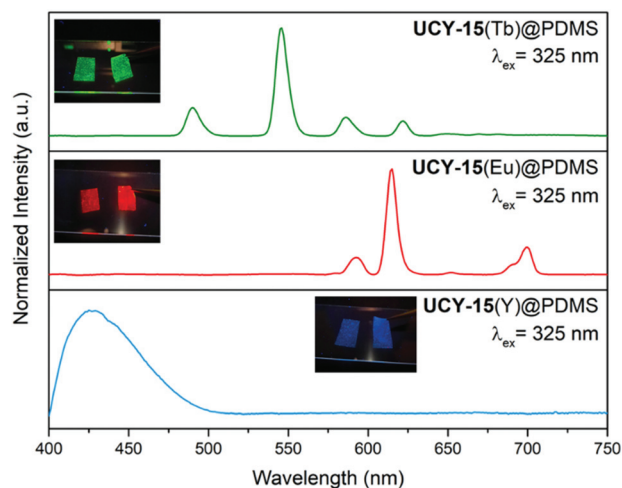


Fig. 5 PL emission spectra ($\lambda_{\text{exc}} = 325 \text{ nm}$) of UCY-15(RE)@PDMS (RE = Y, Eu, Tb) films. Inset: images of UCY-15(RE)@PDMS (RE = Y, Eu, Tb) films exhibiting their characteristic emission (blue, red and green) when irradiated with UV light (300–375 nm).

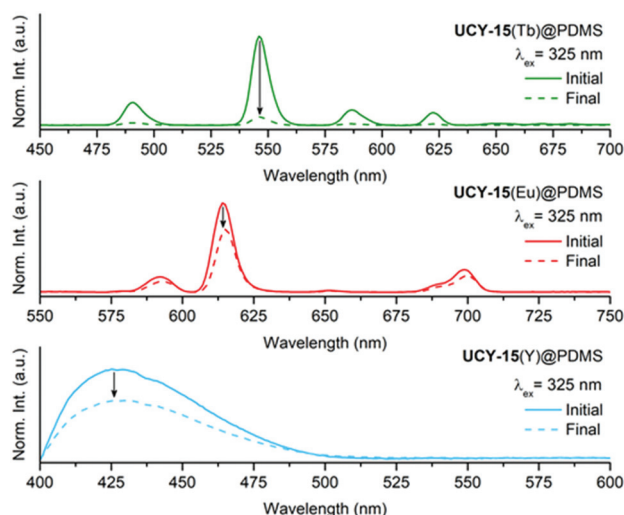


Fig. 6 PL emission spectra ($\lambda_{\text{exc.}} = 325 \text{ nm}$) of UCY-15(RE)@PDMS (RE = Y, Eu, Tb) films before (solid line) and after (dashed line) exposure to TNT saturated vapours.

The PL quenching (%) was quantified as $(1 - I/I_0) \times 100$, where I_0 is the maximum PL intensity for each MOF, and I is the PL intensity at the same wavelength after exposure to saturated vapours of the analyte. Specifically, for UCY-15(RE)@PDMS films, the PL quenching was calculated as $\sim 35\%$, $\sim 32\%$ and $\sim 90\%$, for the Y^{3+} , Eu^{3+} and Tb^{3+} MOF-based materials, respectively.

The observed quenching can be attributed to the electron-withdrawing nature of the TNT molecule that behaves as a π -electron acceptor, quenching the PL by an energy transfer from the excited state of the ligand to the analyte. This mechanism is based on the presence of nitro groups ($-\text{NO}_2$) in its

structure. A plausible explanation of the different percentage of PL quenching obtained for the three UCY-15(RE)@PDMS films can be found in a recent work by A. Gamonal *et al.*⁸¹ where it was demonstrated that divergent alterations of the PL emission of Tb and Eu MOFs, in the presence of NO₂ gas, took place due to a downshift of the excited T₁ energy state of the ligand after adsorption of the analyte. In any case and taking into account the low vapour pressure of TNT,⁸² these results illustrate the high sensitivity of our sensing materials.

The capability of UCY-15(RE)@PDMS films (Y³⁺, Eu³⁺ and Tb³⁺) to detect a number of different analytes exhibiting various chemical moieties and belonging to different target groups including explosives such as nitro-compounds (TNP, DNT, DNB, DMNB) and a strong oxidant improvised explosive (TATP) as well as volatile organic compounds such as alcohols (methanol), aldehydes (hexanal), amines (methylamine), polar solvents (chloroform) and non-polar solvents (toluene) was investigated aiming to obtain information concerning the selectivity of the sensing materials. The corresponding spectra before and after their exposure to the target analytes are provided in ESI (Fig. S21–S23[†]). These studies revealed that the three MOFs are sensitive to most of the selected analytes. To facilitate the visualization of the specific spectral changes by magnifying the resulting modifications upon addition of the analytes to the UCY-15(RE)@PDMS (RE = Y, Eu, Tb) films, the emission spectra before and after exposure were subtracted and the obtained differences were squared. The corresponding results are shown in Fig. 7. As can be seen, a different spectral change (response) is obtained for each MOF and analyte, indicating that a proper combination of the sensing responses can produce selective patterns for the identification of each analyte.

These investigations revealed a variety of spectral changes of UCY-15(RE)@PDMS (RE = Y, Eu, Tb) films for a series of analytes highlighting the capability of these materials to detect several explosives as well as volatile organic compounds. Apart from the electron-withdrawing nature of oxidizing species that induces a charge transfer from the ligand, other types of interactions including metal coordination (through analyte functional groups), π - π interactions, acid–base interactions, hydrogen-bonding interactions, van der Waals interactions and physical adsorption, should be considered in order to explain the different spectral changes observed for the different analytes.^{25,68,83} Since SDBA²⁻ can sensitize both Eu³⁺ and Tb³⁺ ions (*vide supra*) it was decided to combine the emission profiles of UCY-15(Y), UCY-15(Eu) and UCY-15(Tb) into one material. This was considered to be beneficial for gas sensing studies because it would allow to include all visible spectral information in one MOF, obtaining an advanced material for chemical sensing. To achieve this, a series of trimetallic UCY-15(Y_{100-x-y}Eu_xTb_y) (x, y = 5, 7.5, 10) analogues were synthesized by adding calculated amounts of Eu³⁺ and Tb³⁺ salts in the reaction mixtures (see Experimental section).

Due to the similarity in the chemical properties of Y³⁺ and rare earth ions, the dopant Eu³⁺ and Tb³⁺ ions occupy random positions within the metal SBUs of UCY-15(Y_{100-x-y}Eu_xTb_y)

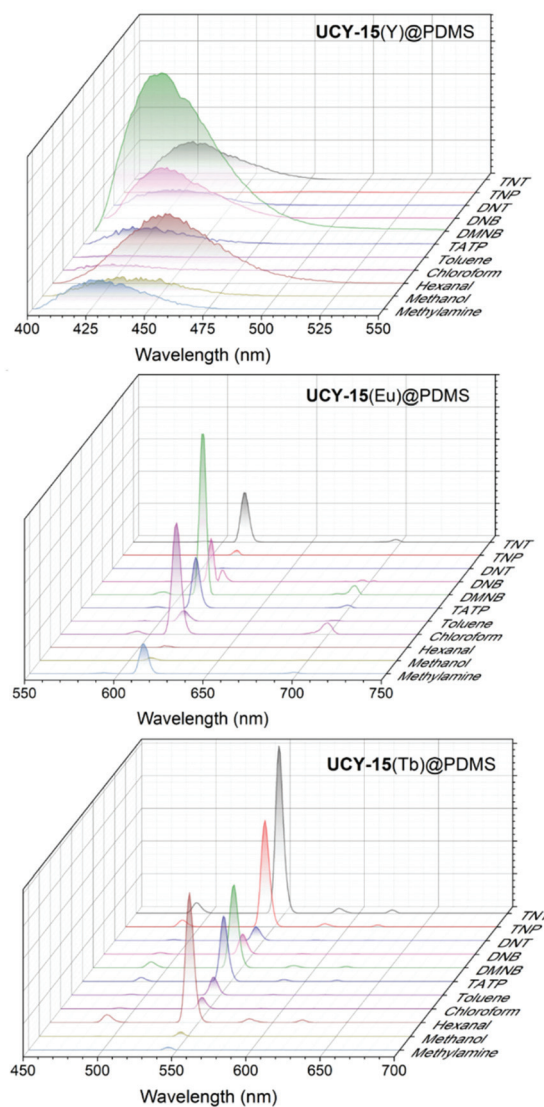


Fig. 7 Squared difference spectra of UCY-15(RE)@PDMS (RE = Y, Eu, Tb) films exposed to saturated vapours of the selected analytes indicated in the corresponding graphs.

(x, y = 5, 7.5, 10). pXRD studies revealed that the isolated microcrystalline powder products of UCY-15(Y_{100-x-y}Eu_xTb_y) (x, y = 5, 7.5, 10) are crystalline and isomorphous to the parent compound UCY-15(Y) (Fig. S24[†]). This strategy for the introduction of new PL centers within a MOF has been demonstrated to be successful in a plethora of lanthanide-based materials.^{13,14,25,53} The emission spectra of the trimetallic analogues UCY-15(Y_{100-x-y}Eu_xTb_y) (x, y = 5, 7.5, 10), upon irradiation at 325 nm (SDBA²⁻ excitation wavelength), contain the PL features of all emissive sites (Fig. S25[†]). Notably, the Eu³⁺ emission bands (e.g. these at 613 nm and 699 nm) are more intense compared to the Tb³⁺ ones. The relative intensity of the emission bands of the rare earth ions in UCY-15 (Y_{100-x-y}Eu_xTb_y) (x, y = 5, 7.5, 10) depends on the energy transfer processes that take place upon excitation of the compounds. The facts that SDBA²⁻ ligand can sensitize both Eu³⁺

and Tb^{3+} ions and energy transfer from Tb^{3+} ions towards Eu^{3+} ions may occur, allow the tuning of the colour of these trimetallic analogues by varying the ratio of the rare earth ions.^{84,85} White light emission is demonstrated by **UCY-15** ($\text{Y}_{87.5}\text{Eu}_{7.5}\text{Tb}_5$) in the CIE (Commission Internationale de l'Éclairage) diagram where each PL spectra is converted to cartesian coordinates on the specified plot. Specifically, **UCY-15** ($\text{Y}_{87.5}\text{Eu}_{7.5}\text{Tb}_5$) coordinates lie in the center of the CIE plot ($x = 0.339$, $y = 0.337$) indicating that this analogue is capable of emitting white light (Fig. S26 and Table S4†). Digital photographs of **UCY-15**(Eu), **UCY-15**($\text{Y}_{100-x-y}\text{Eu}_x\text{Tb}_y$) ($x, y = 5, 7.5, 10$) and **UCY-15**(Tb) under a conventional UV lamp operating at ~ 365 nm indicate that the colour of the doped compounds matches the colour calculated from the CIE plot (Fig. S27†).

SEM-EDX mapping images of all the trimetallic combinations are shown in Fig. S28.† As can be observed, the images reveal a homogeneous distribution of the three RE^{3+} ions (Y, Eu and Tb) in all cases. The RE^{3+} ions (Y, Eu and Tb) ratios in the trimetallic compounds, determined by EDX studies and summarized in Table S5,† are in accordance with the targeted ratios.

Processing the trimetallic MOFs into MMMs gave rise to well distributed embedded crystals with a combined emission colour as depicted in Fig. S29.† Given the well-balanced intensity of the PL bands of the **UCY-15**($\text{Y}_{87.5}\text{Eu}_5\text{Tb}_{7.5}$)@PDMS, this MOF was selected to test the sensing capability of the trimetallic derivatives. As can be seen in Fig. 8a, the emission spectra of the **UCY-15**($\text{Y}_{87.5}\text{Eu}_5\text{Tb}_{7.5}$)@PDMS films maintain the same profile as the microcrystalline powder of the corresponding trimetallic analogue (Fig. S25†). The **UCY-15**($\text{Y}_{87.5}\text{Eu}_5\text{Tb}_{7.5}$)@PDMS films were exposed to saturated vapours of the same group of analytes as in the case of the monometallic MOFs (**UCY-15**(RE), (RE = Y, Eu, Tb) to investigate their sensing capabilities. Fig. S30 and S31† show the corresponding PL spectra before and after 5 min and saturation exposures respectively. As expected, in both cases the presence of the different analytes induces spectral changes in the PL features of each component of the trimetallic MOF. Moreover, the observed changes are different depending on the selected analyte. In order to concentrate this information in only one representation, we have created a recognition pattern by calculating the squared difference spectra for each analyte from Fig. S30† and representing all of them together in a heat map (Fig. 8b). The image consists of 11 columns corresponding to the 11 analytes included in this study. Every column shows the squared difference of the corresponding emission spectrum, before and after exposure, in a colour scale from blue to red, where blue corresponds to no change and the red colour represents the most prominent change detected. The wavelength grows from down to top in each column. Through this representation, the band shifts and PL intensity changes produced by the different analytes can be easily distinguished, giving specific information about the compound to be identified.

Focusing on nitro-compounds, it can be seen from Fig. 8b that there are quite different responses of the **UCY-15**($\text{Y}_{87.5}\text{Eu}_5\text{Tb}_{7.5}$)@PDMS film upon exposure to these analytes

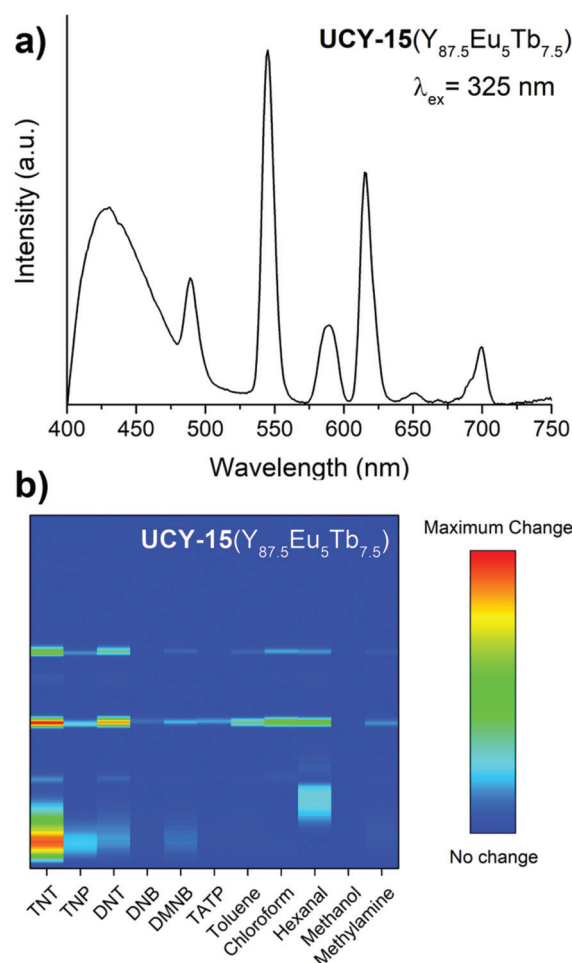


Fig. 8 (a) PL emission spectrum of a **UCY-15**($\text{Y}_{87.5}\text{Eu}_5\text{Tb}_{7.5}$)@PDMS film ($\lambda_{\text{exc.}} = 325$ nm) and (b) colour map of the squared difference spectra of **UCY-15**($\text{Y}_{87.5}\text{Eu}_5\text{Tb}_{7.5}$)@PDMS films after exposure to saturated vapours of the indicated analytes.

unlike their similar chemical structure. As explained above, this behaviour is attributed to the different electron-withdrawing capability of these analytes, and the different quenching degrees upon exposure to them may be explained by their potential redox values; -0.4 V for TNP,⁸⁶ -0.7 V for TNT,⁶⁰ -0.9 V for DNB,⁶⁰ -1.0 V for DNT⁶⁰ and -2.0 V for DMNB.⁸⁷

According to this, the greater the redox potential, the greater the electron-withdrawing nature and, consequently, a more significant response.^{15,16,88–90} The PL quenching, as well as the response normalised by the gas concentration, are summarised in Table S6 in the ESI.† The sensitivity order (TNP > TNT > DNT > DNB > DMNB) obtained from these results agrees with previous studies reported in ethanol solution and gas media.^{15,60,91} A fact supporting the proposed mechanism for the sensing response towards the nitroaromatics is that DMNB does not have a good electron-withdrawing capability, and, therefore, a high response is not expected. Other analytes also exhibit unique changes, as shown in Fig. 8. Overall, this study establishes materials based on microporous trimetallic

RE³⁺ MOFs as an ideal platform for the selective detection of a wide range of analytes since they combine the spectral features of Tb³⁺, Eu³⁺ and the organic bridging ligand that can be modified by a different degree upon exposure to various analytes.

Conclusions

A rare example of 2-dimensional RE³⁺ MOFs based on an eight-connected hexanuclear (RE³⁺)₆ SBU is reported with the formula [RE₆(μ₃-OH/F)₈(SDBA)₄(NO₃)₂(H₂O)₆]_n (UCY-15(RE) RE: Y, Eu, Gd, Tb, Dy, Ho, Er). Gas sorption studies revealed that UCY-15(Y) has a microporous structure and exhibits a moderate internal surface area. Photoluminescence studies on microcrystalline powder samples indicated that SDBA²⁻ anion can effectively sensitize both Eu³⁺ and Tb³⁺ ions. Sensing studies on thin films of UCY-15(RE) (RE: Y, Eu, Tb) embedded in PDMS revealed a variety of different PL responses upon exposure to saturated vapours of various nitro-compounds and VOCs indicating the capability of these materials to detect a wide range of analytes. A series of trimetallic analogues UCY-15(Y_{100-x-y}Eu_xTb_y) (x, y = 5, 7.5, 10) were synthesized aiming to materials that combine the PL signals of UCY-15(Y), UCY-15(Eu) and UCY-15(Tb) MOFs and exhibit superior gas sensing properties. Photoluminescence studies revealed that the UCY-15(Y_{100-x-y}Eu_xTb_y) family is a tunable platform in terms of its PL features with some of these analogues exhibiting the PL signals of Tb³⁺, Eu³⁺ and SDBA²⁻ ions and that white light emission was achieved for one of the analogues (UCY-15(Y_{87.5}Eu₅Tb_{7.5})). The analogue UCY-15(Y_{87.5}Eu₅Tb_{7.5}) that was shown to exhibit a well-balanced intensity of the PL bands of Tb³⁺, Eu³⁺ and SDBA²⁻ ions was selected to fabricate thin films and investigate their sensing capability. The visualization of the squared difference PL spectra before and after exposure of UCY-15(Y_{87.5}Eu₅Tb_{7.5})@PDMS films to saturated vapours of nitro compounds and VOCs in a 2D map allowed the generation of recognition patterns for each analyte. Overall, this work indicates the capability of microporous 2D RE³⁺ MOFs to detect a wide range of analytes since due to their 2D nature exhibit highly accessible metal sites and functional groups and can lead to a variety of PL responses upon interaction with organic molecules. It also demonstrates trimetallic UCY-15(Y_{100-x-y}Eu_xTb_y) analogues as a tunable MOF platform that can facilitate the detection of a wide range of analytes.

Conflicts of interest

There are no conflicts to declare.

Acknowledgements

This work was funded under the M-ERA.NET Call 2019 and the Republic of Cyprus through the Research and Innovation

Foundation (contract no: P2P/M-ERA.NET/0319/0005; Acronym: SALMOS). This research has been also funded by the Spanish AEI/MCIN/10.13039/501100011033 within the NextGenerationEU/PRTR funds through the projects PCI2020-112241 (M-ERA.NET 2019 project7106, SALMOS) and PID2019-110430 GB-C22 (ADLIGHT). European Regional Development Fund (80%) and Andalusian CTEICU/JA in the framework of the Operative Programme FEDER-Andalucia 2014–2020 through projects P20_01258 (objective 01) and UPO-1381028 (objective 1.2.3.) also contributed to the present research. We also thank the laboratory of materials characterization INMALAB of Universidad Pablo de Olavide for experiments and technical support.

References

- 1 P. Silva, S. M. F. Vilela, J. P. C. Tomé and F. A. Almeida Paz, Multifunctional metal–organic frameworks: from academia to industrial applications, *Chem. Soc. Rev.*, 2015, **44**, 6774.
- 2 A. Kumar, D. G. Madden, M. Lusi, K.-J. Chen, E. A. Daniels, T. Curtin, J. J. Perry IV and M. J. Zaworotko, Direct Air Capture of CO₂ by Physisorbent Materials, *Angew. Chemie Int. Ed.*, 2015, **54**, 14372.
- 3 S. Zheng, T. Wu, J. Zhang, M. Chow, R. A. Nieto, P. Feng and X. Bu, Porous Metal Carboxylate Boron Imidazolate Frameworks, *Angew. Chemie Int. Ed.*, 2010, **49**, 5362.
- 4 B. Li, H.-M. Wen, W. Zhou, J. Q. Xu and B. Chen, Porous Metal-Organic Frameworks: Promising Materials for Methane Storage, *Chem*, 2016, **1**, 557.
- 5 H. Li, K. Wang, Y. Sun, C. T. Lollar, J. Li and H.-C. Zhou, Recent advances in gas storage and separation using metal–organic frameworks, *Mater. Today*, 2018, **21**, 108.
- 6 S. L. Anderson, P. G. Boyd, A. Gładysiak, T. N. Nguyen, R. G. Palgrave, D. Kubicki, L. Emsley, D. Bradshaw, M. J. Rosseinsky, B. Smit and K. C. Stylianou, Nucleobase pairing and photodimerization in a biologically derived metal-organic framework nanoreactor, *Nat. Commun.*, 2019, **10**, 1612.
- 7 A. Dhakshinamoorthy, Z. Li and H. Garcia, Catalysis and photocatalysis by metal organic frameworks, *Chem. Soc. Rev.*, 2018, **47**, 8134.
- 8 H. Wang, W. P. Lustig and J. Li, Sensing and capture of toxic and hazardous gases and vapors by metal–organic frameworks, *Chem. Soc. Rev.*, 2018, **47**, 4729.
- 9 E. A. Dolgoplova, A. M. Rice, C. R. Martin and N. B. Shustova, Photochemistry and photophysics of MOFs: steps towards MOF-based sensing enhancements, *Chem. Soc. Rev.*, 2018, **47**, 4710.
- 10 J. Li, X. Wang, G. Zhao, C. Chen, Z. Chai, A. Alsaedi, T. Hayat and X. Wang, Metal–organic framework-based materials: superior adsorbents for the capture of toxic and radioactive metal ions, *Chem. Soc. Rev.*, 2018, **47**, 2322.
- 11 M. Eddaoudi, D. B. Moler, H. Li, B. Chen, T. M. Reineke, M. O’Keeffe and O. M. Yaghi, Modular Chemistry: Secondary Building Units as a Basis for the Design of

- Highly Porous and Robust Metal–Organic Carboxylate Frameworks, *Acc. Chem. Res.*, 2001, **34**, 319.
- 12 C. Pagis, M. Ferbinteanu, G. Rothenberg and S. Tanase, Lanthanide-Based Metal Organic Frameworks: Synthetic Strategies and Catalytic Applications, *ACS Catal.*, 2016, **6**, 6063.
 - 13 Y. Yang, L. Chen, F. Jiang, M. Yu, X. Wan, B. Zhang and M. Hong, A family of doped lanthanide metal–organic frameworks for wide-range temperature sensing and tunable white light emission, *J. Mater. Chem. C*, 2017, **5**, 1981.
 - 14 D. K. Singha, P. Majee, S. K. Mondal and P. Mahata, Visible detection of explosive nitroaromatics facilitated by a large Stokes shift of luminescence using europium and terbium doped yttrium based MOFs, *RSC Adv.*, 2015, **5**, 102076.
 - 15 F. G. Moscoso, J. Almeida, A. Sousaraei, T. Lopes-Costa, A. M. G. Silva, J. Cabanillas-Gonzalez, L. Cunha-Silva and J. M. Pedrosa, A lanthanide MOF immobilized in PMMA transparent films as a selective fluorescence sensor for nitroaromatic explosive vapours, *J. Mater. Chem. C*, 2020, **8**, 3626.
 - 16 F. G. Moscoso, J. Almeida, A. Sousaraei, T. Lopes-Costa, A. M. G. Silva, J. Cabanillas-Gonzalez, L. Cunha-Silva and J. M. Pedrosa, Luminescent MOF crystals embedded in PMMA/PDMS transparent films as effective NO₂ gas sensors, *Mol. Syst. Des. Eng.*, 2020, **5**, 1048.
 - 17 Y. Cui, B. Chen and G. Qian, Lanthanide metal-organic frameworks for luminescent sensing and light-emitting applications, *Coord. Chem. Rev.*, 2014, **273–274**, 76.
 - 18 S. A. Diamantis, A. Margariti, A. D. Pournara, G. S. Papaefstathiou, M. J. Manos and T. Lazarides, Luminescent metal–organic frameworks as chemical sensors: common pitfalls and proposed best practices, *Inorg. Chem. Front.*, 2018, **5**, 1493.
 - 19 W. P. Lustig, S. Mukherjee, N. D. Rudd, A. V. Desai, J. Li and S. K. Ghosh, Metal–organic frameworks: functional luminescent and photonic materials for sensing applications, *Chem. Soc. Rev.*, 2017, **46**, 3242.
 - 20 J. Della Rocca, D. Liu and W. Lin, Nanoscale Metal–Organic Frameworks for Biomedical Imaging and Drug Delivery, *Acc. Chem. Res.*, 2011, **44**, 957.
 - 21 B. Yan, Luminescence response mode and chemical sensing mechanism for lanthanide-functionalized metal–organic framework hybrids, *Inorg. Chem. Front.*, 2021, **8**, 201.
 - 22 J. Rocha, C. D. S. Brites and L. D. Carlos, Lanthanide Organic Framework Luminescent Thermometers, *Chem. – A Eur. J.*, 2016, **22**, 14782.
 - 23 T. Xia, Z. Shao, X. Yan, M. Liu, L. Yu, Y. Wan, D. Chang, J. Zhang and D. Zhao, Tailoring the triplet level of isomorphous Eu/Tb mixed MOFs for sensitive temperature sensing, *Chem. Commun.*, 2021, **57**, 3143.
 - 24 F. M. Ebrahim, T. N. Nguyen, S. Shyshkanov, A. Gładysiak, P. Favre, A. Zacharia, G. Itkos, P. J. Dyson and K. C. Stylianou, Selective, Fast-Response, and Regenerable Metal–Organic Framework for Sampling Excess Fluoride Levels in Drinking Water, *J. Am. Chem. Soc.*, 2019, **141**, 3052.
 - 25 Y. Su, J. Yu, Y. Li, S. F. Z. Phua, G. Liu, W. Q. Lim, X. Yang, R. Ganguly, C. Dang, C. Yang and Y. Zhao, Versatile bi-metallic lanthanide metal-organic frameworks for tunable emission and efficient fluorescence sensing, *Commun. Chem.*, 2018, **1**, 12.
 - 26 H. Xu, B. Zhai, C.-S. Cao and B. Zhao, A Bifunctional Europium–Organic Framework with Chemical Fixation of CO₂ and Luminescent Detection of Al³⁺, *Inorg. Chem.*, 2016, **55**, 9671.
 - 27 H. Xu, H.-C. Hu, C.-S. Cao and B. Zhao, Lanthanide Organic Framework as a Regenerable Luminescent Probe for Fe³⁺, *Inorg. Chem.*, 2015, **54**, 4585.
 - 28 H. Xu, C.-S. Cao, X.-M. Kang and B. Zhao, Lanthanide-based metal–organic frameworks as luminescent probes, *Dalton Trans.*, 2016, **45**, 18003.
 - 29 Y. Gao, P. Jing, N. Yan, M. Hilbers, H. Zhang, G. Rothenberg and S. Tanase, Dual-mode humidity detection using a lanthanide-based metal–organic framework: towards multifunctional humidity sensors, *Chem. Commun.*, 2017, **53**, 4465.
 - 30 P. Samanta, A. V. Desai, S. Let and S. K. Ghosh, Advanced Porous Materials for Sensing, Capture and Detoxification of Organic Pollutants toward Water Remediation, *ACS Sustainable Chem. Eng.*, 2019, **7**, 7456.
 - 31 R. Fu, S. Hu and X. Wu, Rapid and sensitive detection of nitroaromatic explosives by using new 3D lanthanide phosphonates, *J. Mater. Chem. A*, 2017, **5**, 1952.
 - 32 Z. Hu, B. J. Deibert and J. Li, Luminescent metal-organic frameworks for chemical sensing and explosive detection, *Chem. Soc. Rev.*, 2014, **43**, 5815.
 - 33 G.-L. Law, R. Pal, L. O. Palsson, D. Parker and K.-L. Wong, Responsive and reactive terbium complexes with an azaxanthone sensitizer and one naphthyl group: applications in ratiometric oxygen sensing in vitro and in regioselective cell killing, *Chem. Commun.*, 2009, 7321.
 - 34 N. B. Shustova, A. F. Cozzolino, S. Reineke, M. Baldo and M. Dincă, Selective Turn-On Ammonia Sensing Enabled by High-Temperature Fluorescence in Metal–Organic Frameworks with Open Metal Sites, *J. Am. Chem. Soc.*, 2013, **135**, 13326.
 - 35 Z. Dou, J. Yu, Y. Cui, Y. Yang, Z. Wang, D. Yang and G. Qian, Luminescent Metal–Organic Framework Films As Highly Sensitive and Fast-Response Oxygen Sensors, *J. Am. Chem. Soc.*, 2014, **136**, 5527.
 - 36 W.-P. Ma and B. Yan, Lanthanide functionalized MOF thin films as effective luminescent materials and chemical sensors for ammonia, *Dalton Trans.*, 2020, **49**, 15663.
 - 37 J.-N. Hao and B. Yan, A dual-emitting 4d–4f nanocrystalline metal–organic framework as a self-calibrating luminescent sensor for indoor formaldehyde pollution, *Nanoscale*, 2016, **8**, 12047.
 - 38 J. E. Ellis, S. E. Crawford and K.-J. Kim, Metal–organic framework thin films as versatile chemical sensing materials, *Mater. Adv.*, 2021, **2**, 6169.

- 39 A. Sousaraei, C. Queirós, F. G. Moscoso, T. Lopes-Costa, J. M. Pedrosa, A. M. G. Silva, L. Cunha-Silva and J. Cabanillas-Gonzalez, Subppm Amine Detection via Absorption and Luminescence Turn-On Caused by Ligand Exchange in Metal Organic Frameworks, *Anal. Chem.*, 2019, **91**, 15853.
- 40 A. Sousaraei, C. Queirós, F. G. Moscoso, A. M. G. Silva, T. Lopes-Costa, J. M. Pedrosa, L. Cunha-Silva and J. Cabanillas-Gonzalez, Reversible Protonation of Porphyrinic Metal-Organic Frameworks Embedded in Nanoporous Polydimethylsiloxane for Colorimetric Sensing, *Adv. Mater. Interfaces*, 2021, **8**, 2001759.
- 41 J. H. Cavka, S. Jakobsen, U. Olsbye, N. Guillou, C. Lamberti, S. Bordiga and K. P. Lillerud, A New Zirconium Inorganic Building Brick Forming Metal Organic Frameworks with Exceptional Stability, *J. Am. Chem. Soc.*, 2008, **130**, 13850.
- 42 Y. Bai, Y. Dou, L.-H. Xie, W. Rutledge, J.-R. Li and H.-C. Zhou, Zr-based metal-organic frameworks: design, synthesis, structure, and applications, *Chem. Soc. Rev.*, 2016, **45**, 2327.
- 43 S. Yuan, L. Feng, K. Wang, J. Pang, M. Bosch, C. Lollar, Y. Sun, J. Qin, X. Yang, P. Zhang, Q. Wang, L. Zou, Y. Zhang, L. Zhang, Y. Fang, J. Li and H. Zhou, Stable Metal-Organic Frameworks: Design, Synthesis, and Applications, *Adv. Mater.*, 2018, **30**, 1704303.
- 44 Z. Chen, S. L. Hanna, L. R. Redfern, D. Alezi, T. Islamoglu and O. K. Farha, Reticular chemistry in the rational synthesis of functional zirconium cluster-based MOFs, *Coord. Chem. Rev.*, 2019, **386**, 32.
- 45 D.-X. Xue, A. J. Cairns, Y. Belmabkhout, L. Wojtas, Y. Liu, M. H. Alkordi and M. Eddaoudi, Tunable Rare-Earth fcu-MOFs: A Platform for Systematic Enhancement of CO₂ Adsorption Energetics and Uptake, *J. Am. Chem. Soc.*, 2013, **135**, 7660.
- 46 T. Islamoglu, D. Ray, P. Li, M. B. Majewski, I. Akpınar, X. Zhang, C. J. Cramer, L. Gagliardi and O. K. Farha, From Transition Metals to Lanthanides to Actinides: Metal-Mediated Tuning of Electronic Properties of Isostructural Metal-Organic Frameworks, *Inorg. Chem.*, 2018, **57**, 13246.
- 47 O. A. Ejegbavwo, C. R. Martin, O. A. Olorunfemi, G. A. Leith, R. T. Ly, A. M. Rice, E. A. Dolgoplova, M. D. Smith, S. G. Karakalos, N. Birkner, B. A. Powell, S. Pandey, R. J. Koch, S. T. Misture, H.-C. zur Loye, S. R. Phillpot, K. S. Brinkman and N. B. Shustova, Thermodynamics and Electronic Properties of Heterometallic Multinuclear Actinide-Containing Metal-Organic Frameworks with “Structural Memory”, *J. Am. Chem. Soc.*, 2019, **141**, 11628.
- 48 V. Guillerm, Ł. J. Weseliński, Y. Belmabkhout, A. J. Cairns, V. D’Elia, Ł. Wojtas, K. Adil and M. Eddaoudi, Discovery and introduction of a (3,18)-connected net as an ideal blueprint for the design of metal-organic frameworks, *Nat. Chem.*, 2014, **6**, 673.
- 49 C. Liu, S. V. Eliseeva, T.-Y. Luo, P. F. Muldoon, S. Petoud and N. L. Rosi, Near infrared excitation and emission in rare earth MOFs via encapsulation of organic dyes, *Chem. Sci.*, 2018, **9**, 8099.
- 50 N. Panagiotou, I. Liatsou, A. Pournara, G. K. Angeli, R. M. Giappa, E. Tylianakis, M. J. Manos, G. E. Froudakis, P. N. Trikalitis, I. Pashalidis and A. J. Tasiopoulos, Water-stable 2-D Zr MOFs with exceptional UO₂²⁺ sorption capability, *J. Mater. Chem. A*, 2020, **8**, 1849.
- 51 J. Duan, Y. Li, Y. Pan, N. Behera and W. Jin, Metal-organic framework nanosheets: An emerging family of multifunctional 2D materials, *Coord. Chem. Rev.*, 2019, **395**, 25.
- 52 C. Tan, X. Cao, X.-J. Wu, Q. He, J. Yang, X. Zhang, J. Chen, W. Zhao, S. Han, G.-H. Nam, M. Sindoro and H. Zhang, Recent Advances in Ultrathin Two-Dimensional Nanomaterials, *Chem. Rev.*, 2017, **117**, 6225.
- 53 N. Panagiotou, K. Evangelou, A. Psalti, N. Varnava, G. K. Angeli, P. N. Trikalitis, J. C. Plakatouras, T. Lazarides and A. J. Tasiopoulos, Improving the Cd²⁺ detection capability of a new anionic rare earth metal-organic framework based on a [RE₆(μ₃-OH)₈]¹⁰⁺ secondary building unit: an ion-exchange approach towards more efficient sensor, *Mol. Syst. Des. Eng.*, 2020, **5**, 1077.
- 54 P. Yi, H. Huang, Y. Peng, D. Liu and C. Zhong, A series of europium-based metal organic frameworks with tuned intrinsic luminescence properties and detection capacities, *RSC Adv.*, 2016, **6**, 111934.
- 55 F. Hu, Z. Di, M. Wu, M. Hong and J. Li, A Robust Multifunctional Eu₆-Cluster Based Framework for Gas Separation and Recognition of Small Molecules and Heavy Metal Ions, *Cryst. Growth Des.*, 2019, **19**, 6381.
- 56 D. F. Sava Gallis, D. J. Vogel, G. A. Vincent, J. M. Rimsza and T. M. Nenoff, NO_x Adsorption and Optical Detection in Rare Earth Metal-Organic Frameworks, *ACS Appl. Mater. Interfaces*, 2019, **11**, 43270.
- 57 X.-Y. Zhao, Y.-S. Shi, M.-L. Pang, W.-N. Zhang and Y.-H. Li, Facile fabrication of Eu-1,4-NDC-fcu-MOF particles for sensing of benzidine, *Main Gr. Chem.*, 2020, **19**, 117.
- 58 J. Feng, T. Liu, J. Shi, S. Gao and R. Cao, Dual-Emitting UiO-66(Zr&Eu) Metal-Organic Framework Films for Ratiometric Temperature Sensing, *ACS Appl. Mater. Interfaces*, 2018, **10**, 20854.
- 59 X.-L. Lv, L. Feng, L.-H. Xie, T. He, W. Wu, K.-Y. Wang, G. Si, B. Wang, J.-R. Li and H.-C. Zhou, Linker Desymmetrization: Access to a Series of Rare-Earth Tetracarboxylate Frameworks with Eight-Connected Hexanuclear Nodes, *J. Am. Chem. Soc.*, 2021, **143**, 2784.
- 60 M. G. Guillén, F. Gámez, J. Roales, T. Lopes-Costa, S. M. A. Pinto, M. J. F. Calvete, M. M. Pereira and J. M. Pedrosa, Molecular-based selection of porphyrins towards the sensing of explosives in the gas phase, *Sensors Actuators B Chem.*, 2018, **260**, 116.
- 61 G. R. Peterson, W. P. Bassett, B. L. Weeks and L. J. Hope-Weeks, Phase pure triacetone triperoxide: The influence of ionic strength, oxidant source, and acid catalyst, *Cryst. Growth Des.*, 2013, **13**, 2307.
- 62 G. Sheldrick, A short history of SHELX, *Acta Crystallogr. Sect. A*, 2008, **64**, 112.

- 63 Oxford Diffraction, *CrysAlis CCD and CrysAlis RED, version p171.38.46*, Oxford Diffraction Ltd, Abingdon, UK, 2017.
- 64 L. J. Farrugia, WinGX suite for small-molecule single-crystal crystallography, *J. Appl. Crystallogr.*, 1999, **32**, 837.
- 65 K. Brandenburg, *Version 2003.2001d*, Crystal Impact GbR, Bonn, Germany, 2006.
- 66 A. L. Spek, Single-crystal structure validation with the program PLATON, *J. Appl. Crystallogr.*, 2003, **36**, 7.
- 67 R. P. Machattos, N. Panagiotou and A. J. Tasiopoulos, Highlighting the structure – directing capability of the functional groups of angular dicarboxylic ligands: New 2-dimensional Cu²⁺ MOFs from analogous synthetic routes, *Polyhedron*, 2021, **205**, 115299.
- 68 P.-Y. Du, W. P. Lustig, S. J. Teat, W. Gu, X. Liu and J. Li, A robust two-dimensional zirconium-based luminescent coordination polymer built on a V-shaped dicarboxylate ligand for vapor phase sensing of volatile organic compounds, *Chem. Commun.*, 2018, **54**, 8088.
- 69 M. Llunell, D. Casanova, J. Cirera, P. Alemany and S. Alvarez, *SHAPE: Program for the stereochemical analysis of molecular fragments by means of continuous shape measures and associated tools*, University of Barcelona, Barcelona, Spain, 2010.
- 70 J. P. Vizuet, M. L. Mortensen, A. L. Lewis, M. A. Wunch, H. R. Firouzi, G. T. McCandless and K. J. Balkus, Fluoro-Bridged Clusters in Rare-Earth Metal–Organic Frameworks, *J. Am. Chem. Soc.*, 2021, **143**, 17995.
- 71 J. I. Deneff, L. E. S. Rohwer, K. S. Butler, N. R. Valdez, M. A. Rodriguez, T. S. Luk and D. F. Sava Gallis, Covert MOF-Based Photoluminescent Tags via Tunable Linker Energetics, *ACS Appl. Mater. Interfaces*, 2022, **14**, 3038.
- 72 C. Glidewell, W. T. A. Harrison, J. N. Low, J. G. Sime and J. L. Wardell, Patterns of soft C—H...O hydrogen bonding in diaryl sulfones, *Acta Crystallogr. Sect. B Struct. Sci.*, 2001, **57**, 190.
- 73 R. G. AbdulHalim, P. M. Bhatt, Y. Belmabkhout, A. Shkurenko, K. Adil, L. J. Barbour and M. Eddaoudi, A Fine-Tuned Metal–Organic Framework for Autonomous Indoor Moisture Control, *J. Am. Chem. Soc.*, 2017, **139**, 10715.
- 74 L. Feng, Y. Wang, K. Zhang, K.-Y. Wang, W. Fan, X. Wang, J. A. Powell, B. Guo, F. Dai, L. Zhang, R. Wang, D. Sun and H.-C. Zhou, Molecular Pivot-Hinge Installation to Evolve Topology in Rare-Earth Metal–Organic Frameworks, *Angew. Chemie Int. Ed.*, 2019, **58**, 16682.
- 75 Y. Wang, L. Feng, W. Fan, K.-Y. Wang, X. Wang, X. Wang, K. Zhang, X. Zhang, F. Dai, D. Sun and H.-C. Zhou, Topology Exploration in Highly Connected Rare-Earth Metal–Organic Frameworks via Continuous Hindrance Control, *J. Am. Chem. Soc.*, 2019, **141**, 6967.
- 76 G. K. Angeli, E. Loukopoulos, K. Kouvidis, A. Bosveli, C. Tsangarakis, E. Tylanakis, G. Froudakis and P. N. Trikalitis, Continuous Breathing Rare-Earth MOFs Based on Hexanuclear Clusters with Gas Trapping Properties, *J. Am. Chem. Soc.*, 2021, **143**, 10250.
- 77 W. Lin, E. Ning, L. Yang, Y. Rao, S. Peng and Q. Li, Snapshots of Postsynthetic Modification in a Layered Metal–Organic Framework: Isometric Linker Exchange and Adaptive Linker Installation, *Inorg. Chem.*, 2021, **60**, 11756.
- 78 Y. Zhang, B. Li, H. Ma, L. Zhang, H. Jiang, H. Song, L. Zhang and Y. Luo, A nanoscaled lanthanide metal–organic framework as a colorimetric fluorescence sensor for dipicolinic acid based on modulating energy transfer, *J. Mater. Chem. C*, 2016, **4**, 7294.
- 79 E. J. Kyprianidou, T. Lazarides, S. Kaziannis, C. Kosmidis, G. Itskos, M. J. Manos and A. J. Tasiopoulos, Single crystal coordinating solvent exchange as a general method for the enhancement of the photoluminescence properties of lanthanide MOFs, *J. Mater. Chem. A*, 2014, **2**, 5258.
- 80 L. Armelao, S. Quici, F. Barigelletti, G. Accorsi, G. Bottaro, M. Cavazzini and E. Tondello, Design of luminescent lanthanide complexes: From molecules to highly efficient photo-emitting materials, *Coord. Chem. Rev.*, 2010, **254**, 487.
- 81 A. Gamonal, C. Sun, A. L. Mariano, E. Fernandez-Bartolome, E. Guerrero-SanVicente, B. Vlasisavljevich, J. Castells-Gil, C. Marti-Gastaldo, R. Poloni, R. Wannemacher, J. Cabanillas-Gonzalez and J. Sanchez Costa, Divergent Adsorption-Dependent Luminescence of Amino-Functionalized Lanthanide Metal–Organic Frameworks for Highly Sensitive NO₂ Sensors, *J. Phys. Chem. Lett.*, 2020, **11**, 3362.
- 82 H. Östmark, S. Wallin and H. G. Ang, Vapor Pressure of Explosives: A Critical Review, Propellants, *Explos. Pyrotech.*, 2012, **37**, 12.
- 83 J. R. Askim, M. Mahmoudi and K. S. Suslick, Optical sensor arrays for chemical sensing: the optoelectronic nose, *Chem. Soc. Rev.*, 2013, **42**, 8649.
- 84 C. Gao, A. M. Kirillov, W. Dou, X. Tang, L. Liu, X. Yan, Y. Xie, P. Zang, W. Liu and Y. Tang, Self-Assembly Synthesis, Structural Features, and Photophysical Properties of Dilanthanide Complexes Derived from a Novel Amide Type Ligand: Energy Transfer from Tb(III) to Eu(III) in a Heterodinuclear Derivative, *Inorg. Chem.*, 2014, **53**, 935.
- 85 Y.-W. Zhao, F.-Q. Zhang and X.-M. Zhang, Single Component Lanthanide Hybrids Based on Metal–Organic Framework for Near-Ultraviolet White Light LED, *ACS Appl. Mater. Interfaces*, 2016, **8**, 24123.
- 86 M. Uchimiya, L. Gorb, O. Isayev, M. M. Qasim and J. Leszczynski, One-electron standard reduction potentials of nitroaromatic and cyclic nitramine explosives, *Environ. Pollut.*, 2010, **158**, 3048.
- 87 M. E. Germain, T. R. Vargo, P. G. Khalifah and M. J. Knapp, Fluorescent Detection of Nitroaromatics and 2,3-Dimethyl-2,3-dinitrobutane (DMNB) by a Zinc Complex: (salophen)Zn, *Inorg. Chem.*, 2007, **46**, 4422.
- 88 J. Roales, J. Pedrosa, M. Guillén, T. Lopes-Costa, P. Castellero, A. Barranco and A. González-Elipse, Free-Base Carboxyphenyl Porphyrin Films Using a TiO₂ Columnar

- Matrix: Characterization and Application as NO₂ Sensors, *Sensors*, 2015, **15**, 11118.
- 89 M. G. Guillén, F. Gámez, B. Suárez, C. Queirós, A. M. G. Silva, Á. Barranco, J. R. Sánchez-Valencia, J. M. Pedrosa and T. Lopes-Costa, Preparation and Optimization of Fluorescent Thin Films of Rosamine-SiO₂/TiO₂ Composites for NO₂ Sensing, *Materials*, 2017, **10**, 124.
- 90 J. Roales, F. Moscoso, F. Gámez, T. Lopes-Costa, A. Sousaraei, S. Casado, J. Castro-Smirnov, J. Cabanillas-Gonzalez, J. Almeida, C. Queirós, L. Cunha-Silva, A. Silva and J. Pedrosa, Preparation of Luminescent Metal-Organic Framework Films by Soft-Imprinting for 2,4-Dinitrotoluene Sensing, *Materials*, 2017, **10**, 992.
- 91 J.-D. Xiao, L.-G. Qiu, F. Ke, Y.-P. Yuan, G.-S. Xu, Y.-M. Wang and X. Jiang, Rapid synthesis of nanoscale terbium-based metal-organic frameworks by a combined ultrasound-vapour phase diffusion method for highly selective sensing of picric acid, *J. Mater. Chem. A*, 2013, **1**, 8745.